Communications in Physics, Vol. 32, No. 3 (2022), pp. 319-329
DOI: https://doi.org/10.15625/0868-3166/16867

OPTICAL PROPERTIES OF ZnO/MoS_2 HETEROSTRUCTURES GROWN BY THERMAL EVAPORATION METHOD

LUU THI HA THU[1,2], DO QUANG TRUNG[3,⋆], MANH TRUNG TRAN[2], NGUYEN TU[3], NGUYEN DUY HUNG[1] AND PHAM THANH HUY[2,†]

[1]*Advanced Institute of Science and Technology (AIST), Hanoi University of Science and Technology (HUST), No. 01 Dai Co Viet, Hanoi 10000, Vietnam*

[2]*Faculty of Materials Science and Engineering, Phenikaa University, Yen Nghia, Ha Dong district, Hanoi 10000, Vietnam*

[3]*Faculty of Fundamental Sciences, Phenikaa University, Yen Nghia, Ha Dong district, Hanoi 10000, Vietnam*

E-mail: ⋆trung.doquang@phenikaa-uni.edu.vn; †huy.phamthanh@phenikaa-uni.edu.vn

Received 6 January 2022; *Accepted for publication 3 June 2022*; *Published 22 June 2022*

Abstract. *Recently, molybdenum sulfide (MoS_2) has attracted significant attention due to its novel two-dimensional layered structure, tunable bandgap, and excellent electronic properties. It is predicted that the combination of MoS_2 and ZnO that forms ZnO/MoS_2 heterostructures could syndicate the unique properties of MoS_2 and ZnO. In this study, ZnO nanowires and ZnO/MoS_2 heterostructure nanowires were successfully grown on Si/Au substrate by a thermal co-evaporation method. It is found that the use of the MoS_2 and ZnO mixture as the source material for evaporation resulted in the growth of ZnO/MoS_2 heterostructure nanowires with smaller diameters compared to that of pure ZnO nanowires grown in the same experimental setup. Photoluminescence (PL) and photoluminescence excitation (PLE) studies reveal a considerable reduction in the intensity of the defect-related visible emissions of the ZnO/MoS_2 heterostructure nanowires, indicating a strong influence of the MoS_2 on the optical properties of the ZnO/MoS_2 products. The visible emission PL intensity reduction is interpreted due to the efficient passivation of the ZnO surface and interface defects by the MoS_2 layer. Additionally, the strong optical absorption in the visible region of MoS_2 and the formation of ZnO/MoS_2 heterostructure with staggered type-II band alignment is supposed to be other causes of this reduction. Gaussian deconvolution of the broad visible emission of ZnO/MoS_2 heterostructures reveals an orange-red emission peaked at 618 nm, which could be attributed to the excess oxygen atoms located at interstitial sites of the ZnO/MoS_2 host lattice.*

Keywords: ZnO nanowires; ZnO/MoS_2 heterostructure nanowires; thermal co-evaporation method; optical properties.

Classification numbers: 64.70.fm; 78.55.Qr; 79.60.Jv.

I. INTRODUCTION

Zinc oxide (ZnO) is a typical semiconductor material that is extensively utilized in various practical applications because of its non-toxicity, low cost, and high stability [1, 2]. Its wide bandgap of 3.37 eV at room temperature makes the wurtzite ZnO structure promising for photonic and optoelectronic applications in the ultraviolet (UV) or blue spectral range [1]. Moreover, its high exciton-binding energy of 60 meV at room temperature allows efficient exciton emissions [2]. According to literature, ZnO doped with transition metals shows promising potential for practical applications [3, 4]. In recent years, transition metal sulfides have been widely investigated in various applications, such as catalysts [5], batteries [6], optoelectronic devices [7], etc. Among them, MoS_2 material is attracting worldwide scientists because its layered structure is similar to graphene, and the difference between the bandgap of hexagonal monolayer (1.9 eV [8]) and that of MoS_2 bulk (1.23 eV [9]). In this structure, while atoms are strongly bonded in the same layer, atoms in neighbored layers only show a weak Van der Waals force [9]. Compared with MoS_2 bulk structures, 2D MoS_2 structures exhibit some unique features, including strong luminescence and magnetic properties [8, 9]. Hence, MoS_2 nanomaterials are extensively applied in electronic and optoelectronic technology [1].

Recent studies have demonstrated that the combination of MoS_2 and ZnO could create some new properties and improve their current features [9–12]. For example, there was a significant enhancement in the photoluminescence intensity of the MoS_2 monolayer when ZnO rods were grown on its surface [13]. Similarly, the presence of MoS_2 on the ZnO surfaces improved the absorption capability of light ranging from UV to the visible region [12] and the separation between charge carriers and their lifetimes [8]. More interestingly, the 2D MoS_2 decorated with ZnO nanorods exhibited new UV and visible emissions [8]. Furthermore, theoretical calculations indicated that the MoS_2 structure could be tunable by changing the crystal surface of ZnO [2]. Until now, ZnO/MoS_2 heterostructures have been mainly fabricated by "liquid exfoliation" [14], a hydrothermal technique [15], or equipped with an evaporation process [8]. ZnO/MoS_2 core-shell structures [16] or heterostructures [10] could be obtained by different methods [17]; however, these structures synthesized by a facile evaporation method and the influence of structural morphology on their optical properties have not been reported yet.

In this study, ZnO/MoS_2 heterostructure nanowires have been successfully grown on Si/Au substrates by a one-step co-evaporation method. The crystalline phase, surface morphology, and optical properties have been investigated by means of X-ray powder diffraction (XRD), field emission scanning electron microscopy (FESEM), Raman, PL, and PLE spectroscopies. We found that incorporating MoS_2 strongly influences the optical properties of the ZnO/MoS_2 heterostructure nanowires by efficiently passivation the interface and surface defects in these heterostructure products.

II. EXPERIMENT

Materials

ZnO (99.99 %), MoO3 (99.97 %), and S (99.98 %) powders were supplied by Sigma-Aldrich. All chemicals were directly used without further purification.

Materials Synthesis

ZnO/MoS_2 heterostructures nanowires were grown by a thermal co-evaporation method. Firstly, a mixture of 0.5 g ZnO, 0.225 g MoO_3, and 0.35 g high purity S powders well prepared by a mortar mixing technique was put in an alumina boat which serves as the evaporation source. The boat was then transferred and placed in the center of a quartz tube furnace (NaberTherm RT 50-250/13). Si/Au substrates, which served as deposition wafers, were placed downstream in the quartz tube. Pure nitrogen (N_2) was used as the carrier gas during the deposition process. Initially, the furnace temperature was set from room temperature to 1100˚C with a step of 10˚C/min, and the N2 gas flow was set at 100 sccm. In the next step, the furnace temperature was increased to 1250˚C with a step of 5˚C/min, then kept for 45 mins for the deposition process. During the deposition process, the flow rate of the N2 gas was reduced to 50 sccm. Finally, the furnace was cooled down to room temperature naturally, and the N2 gas flow was kept constant till cooling down to room temperature. The as-grown product was gray-white layers on the Si/Au substrates. A similar process was also applied using ZnO powder as a source for producing ZnO nanowires.

Characterization

The crystalline structures were studied by X-ray powder diffraction (XRD, Rigaku D/MAX-2500/PC), with CuK_α radiation ($\lambda = 0.154$ nm) and the tube operating current of 40 mA. The surface morphologies and chemical compositions were characterized by FESEM on a JEOL JSM-7600F accompanied by energy-dispersive X-ray spectroscopy (EDS). The Raman spectra were analyzed at room temperature by a Horiba Jobin Yvon MacroRamTM spectrometer using a 780 nm diode laser as excitation (laser power of 7 – 450 mW) with a full-width half-maximum of 0.1 nm. The PL and PLE spectra were investigated by a fluorescence spectrophotometer (NanoLog, Horiba) equipped with a 450 W Xenon lamp.

III. RESULTS AND DISCUSSION

Figure 1 shows the XRD pattern of as-received ZnO and ZnO/MoS_2 samples. All diffraction peaks of ZnO sample at $2\theta = 32.2$, 34.8, 36.7, 48.0, 57.0, and 63.3˚ correspond to the (100), (002), (101), (102), (110), and (103) planes of the hexagonal wurtzite structure of ZnO phase (JCPDS 36-1451) [18, 19]. Besides the presence of the characteristic peaks of the ZnO phase, the XRD pattern of the ZnO/MoS_2 sample displays several peaks at $2\theta = 13.5$, 32.6, 33.7, 39.0, 44.9, 49.6, and 56.3˚, correspond to the (002), (100), (101), (103), (006), (105), and (106) diffraction planes of the hexagonal wurtzite MoS_2 structure (JCPDS 37-1492) [12,20]. These results indicate that the ZnO/MoS_2 heterostructure nanowires are formed in the as-grown sample.

Figure 2 shows the FESEM images of ZnO/MoS_2 and ZnO samples grown at 1100˚C for 45 mins by a thermal evaporation method. As shown in Figs. 2 (a, b), the products found on the Si/Au substrates are nanowires with smooth surfaces and about 600 – 900 nm diameters and lengths of several tens of nanometers. The as-received ZnO/MoS_2 heterostructure nanowires are also nanowires but with smaller diameters ($\sim$ 200 – 400 nm) and rough surfaces, possibly due to the deposition of the MoS_2 on the surface of ZnO nanowires (See Figs. 2 (c,d)).

The chemical elemental composition of ZnO and ZnO/MoS_2 samples was investigated by EDS as shown in Figs. 3 (a,b), respectively. Only two elements, O (53.8 at%) and Zn (46.2 at%), could be detected in Fig. 3a without any additional element. Fig. 3b illustrates that the obtained

ZnO/MoS_2 sample only contains Zn (13.0 at%), O (85.0 at%), S (1.2 at%), and Mo (0.8 at%), besides the appearance of Si substrate, demonstrating the purity of the obtained samples.

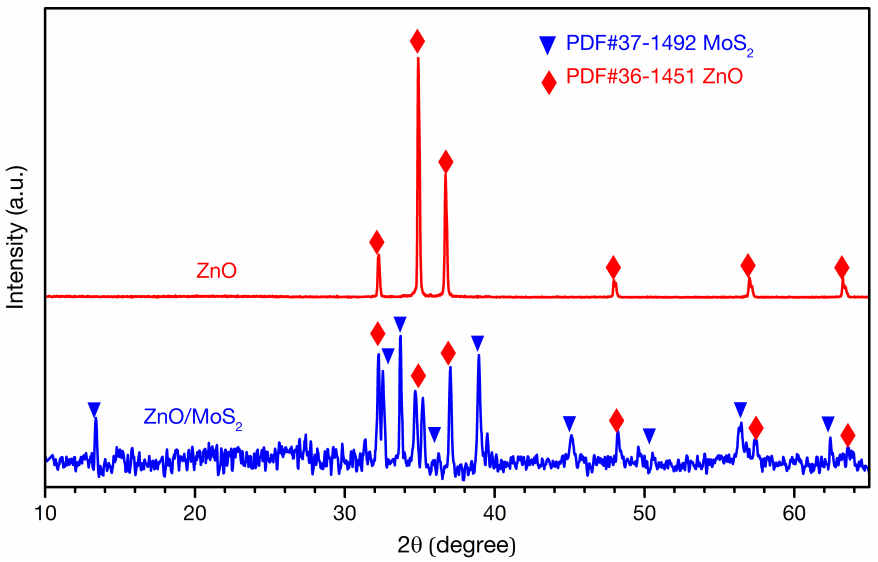

Fig. 1. XRD patterns of ZnO and ZnO/MoS_2 samples grown at 1100˚C for 45 mins by a thermal evaporation method.

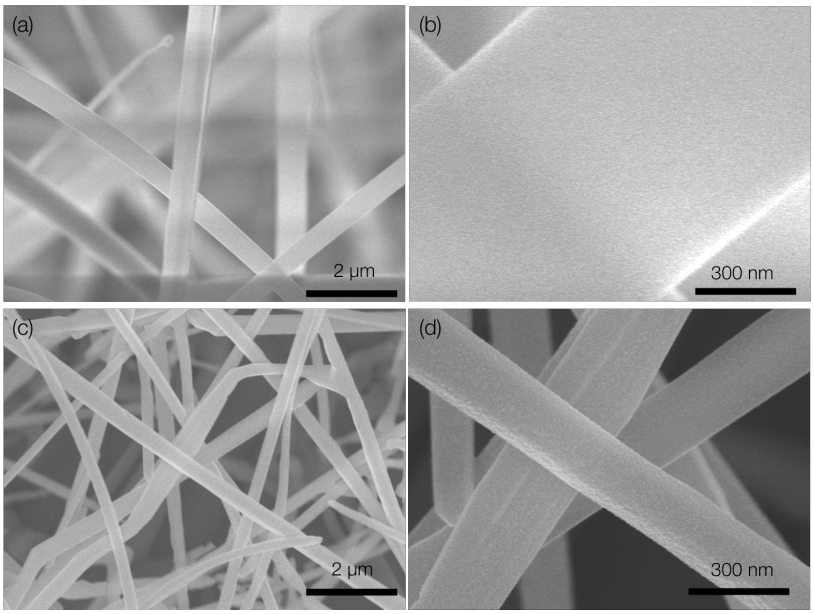

Fig. 2. FESEM images of (a, b) ZnO nanowires and (c, d) ZnO/MoS_2 heterostructure nanowires grown by the thermal evaporation method.

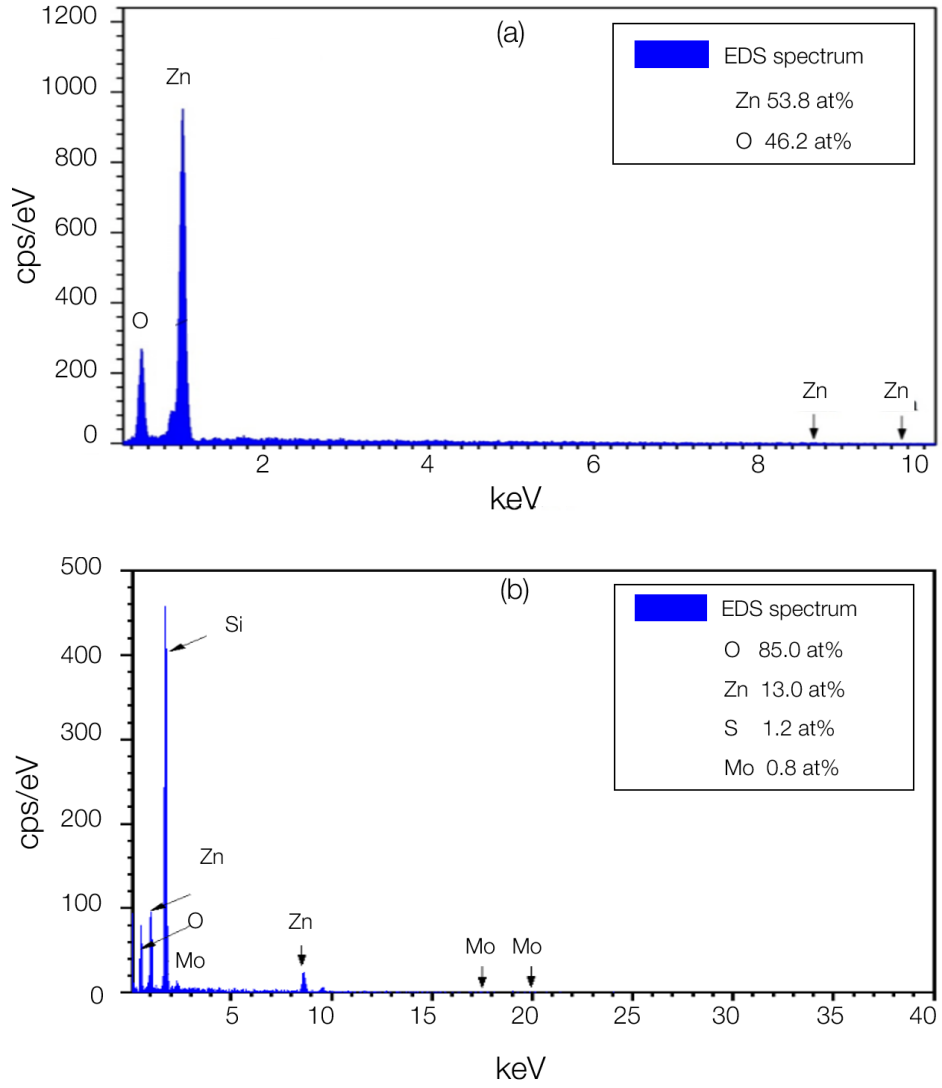

Fig. 3. EDS spectra of (a) ZnO and (b) ZnO/MoS_2 samples grown by the thermal evaporation method.

Figure 4 displays the room-temperature Raman spectra in the range of 100 – 700 cm^{-1} of the ZnO and ZnO/MoS_2 samples. It is shown that the characteristic vibration modes of Si could be clearly observed at 306 and 521 cm^{-1}, contributing to the longitudinal acoustic (LA) and transverse optical (TO) modes of Si [21, 22]. The Raman spectrum of the ZnO sample shows two defined peaks located at 100 and 436 cm^{-1}, corresponding to the two vibrational modes E_2 low (E_2L) and E_2 high (E_2H) of ZnO [23, 24]. For ZnO/MoS_2 sample, the three distinct active modes at 226, 347, and 410 cm^{-1} could be identified as corresponding to the 1T-MoS_2 [25], E^1_{2h} [25], and A_{1g} of MoS_2 [26]. These results confirm the successful growth of ZnO/MoS_2 heterostructures.

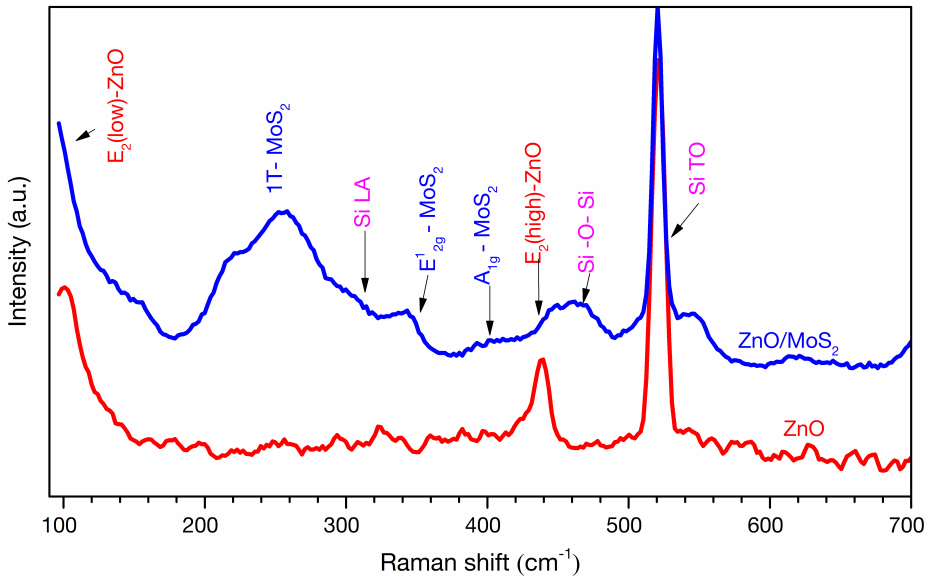

Fig. 4. Raman scattering spectra of (a) ZnO and (b) ZnO/MoS_2 samples grown by a thermal evaporation method.

Photoluminescence and photoluminescence excitation spectroscopies are powerful methods to probe materials' optical and electronic structures [18, 19]. Fig. 5 presents the PLE (Fig. 5a) and the normalized PLE spectra (Fig. 5b) of as-received ZnO and ZnO/MoS_2 samples. It is shown that the PLE intensity of ZnO/MoS_2 heterostructures nanowires is slightly lower than that of the ZnO nanowires. This is possibly caused by the existence of the MoS_2 layer on the surface of the ZnO nanowires. Further, the band edge of the ZnO/MoS_2 heterostructures is blueshifted to higher energy (shorter wavelength) side. The peak at 370 nm is attributed to the near-band-edge (NBE) emission of ZnO, and the peak at 365 nm is related to the ZnO phase in the ZnO/MoS_2 heterostructures [27]. The slight difference between the NBE emission of the ZnO phase in the ZnO/MoS_2 heterostructures and the ZnO nanowires may be caused by the strained lattice generated due to the difference in the primitive cell of ZnO and MoS_2 [11]. Alternatively, it may be due to the passivation of ZnO's interface and surface defects by the MoS_2 layer, as has been reported previously [28].

The PL spectra of ZnO nanowires and ZnO/MoS_2 heterostructures (Fig. 5c) reveal that both samples have two distinguished emission bands. A relatively narrow and weak emission band in the near-ultraviolet region (NUV) peaked at around 380 nm and a broad emission band in the visible from 420 – 700 nm. The NUV band is well-known and could be attributed to the NBE emission of ZnO [29, 30]. The broad visible emission peaked at around 507 nm is defect-related emissions (DE) such as oxygen antisites (OZn), interstitial oxygen (Oi), oxygen vacancy (Vo) in the ZnO nanowires, and ZnO/MoS_2 heterostructures [9, 23]. Further, the visible emission PL intensity of the ZnO/MoS_2 heterostructures was found substantially quenched compared to that of the ZnO nanowires. This result indicates that the formation of the MoS_2 layer has efficiently

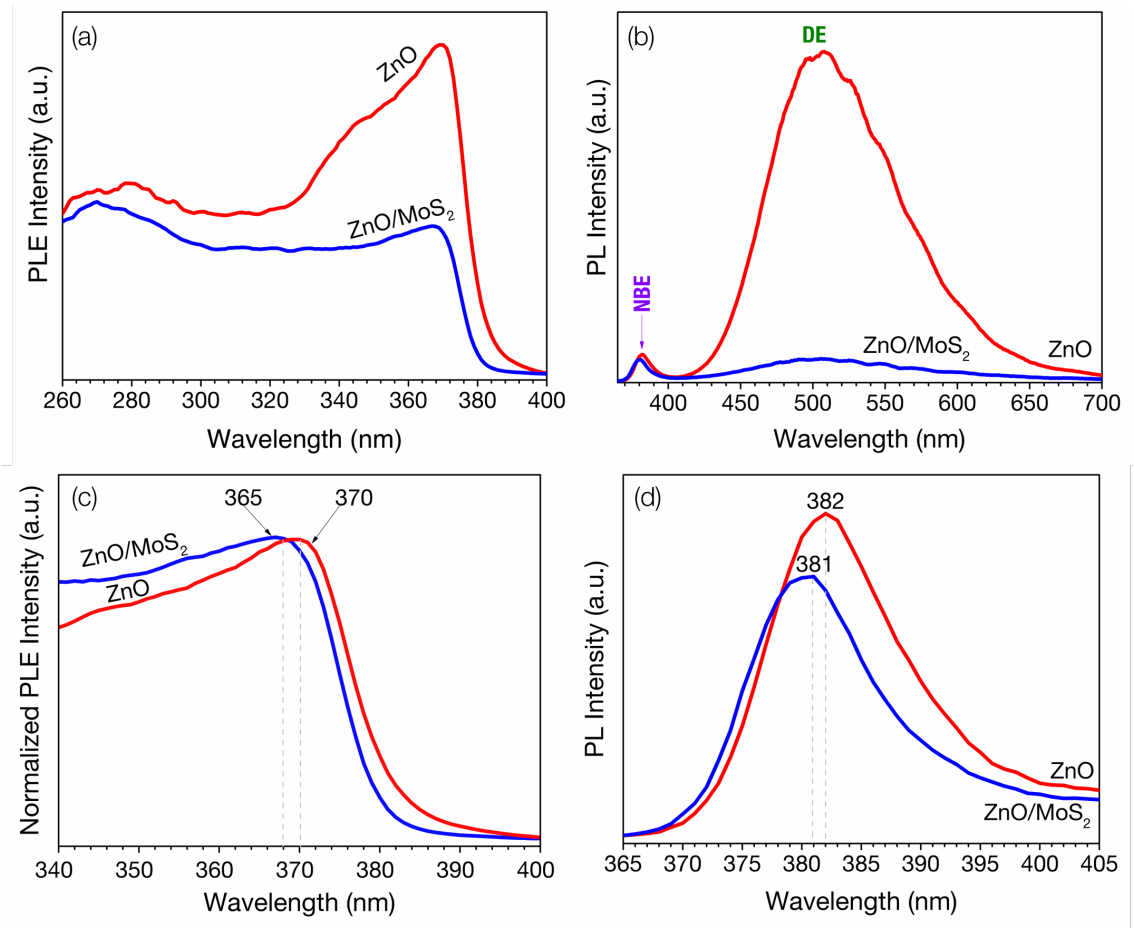

Fig. 5. (a) PLE spectra of the ZnO nanowires and the ZnO/MoS_2 heterostructures nanowires; (b) Comparison of the normalized PLE spectrum of the ZnO and that of the ZnO/MoS_2 heterostructures; (c) PL spectra excited by the 325 nm wavelength of ZnO và ZnO/MoS_2 heterostructures; (d) NBE emissions of ZnO nanowires and ZnO/MoS_2 heterostructures.

passivated the ZnO's interfaces and surface defects, leading to a vast reduction of the PL intensity of defect-related visible emissions.

Additionally, being an n-type semiconductor with a bandgap of 1.2 $\sim$ 1.9 eV, MoS_2 is known to have strong optical absorption in the visible region [9]. Upon incorporation with ZnO to create ZnO/MoS_2 heterostructure, the staggered type-II band alignment is formed at the interface between ZnO and MoS_2 [31]. Under UV excitation, the photogenerated holes in the ZnO are easily moved to the valence band of MoS_2, and the photogenerated electrons in the MoS_2 are also easily transferred to the conduction band of ZnO. These processes significantly reduce the hole/electron capture probability at defects in both the ZnO and MoS_2 phases, thereby reducing the defect-related emissions in the visible, as observed in Fig. 5c.

Figure 5d compares the NBE emission intensity of the ZnO nanowires and ZnO/MoS_2 heterostructures. No improvement in the emission intensity was observed, indicating a negligible influence of heterojunction on the NBE emission of ZnO. Moreover, the NBE emission of ZnO/MoS_2 samples also (381 nm) exhibits a slight "blueshift" towards a shorter wavelength than that of ZnO (382 nm), possibly explained by the effect of surface passivation of MoS_2 in the ZnO/MoS_2 heterostructures [28].

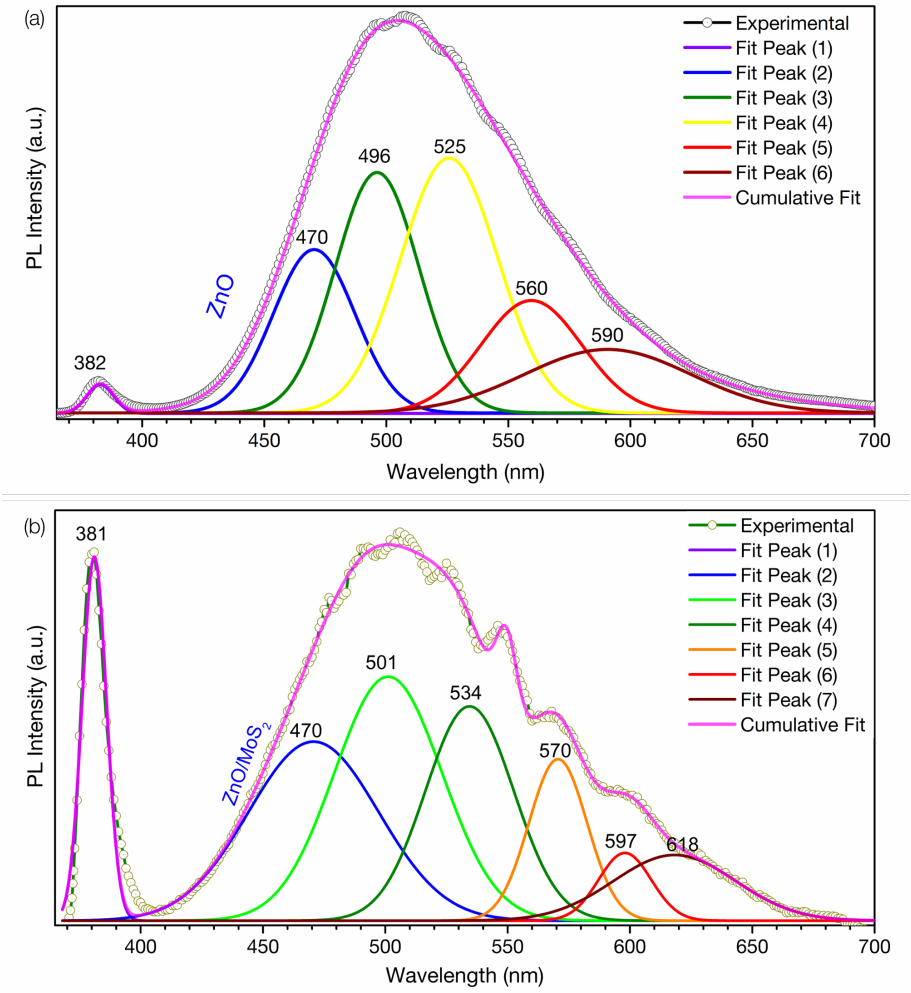

Fig. 6. Gaussian fitting of the visible emissions of (a) ZnO nanowires and (b) ZnO/MoS_2 heterostructures nanowires.

Figures 6 (a, b) show the Gaussian fitting of the broad visible emission of ZnO and ZnO/MoS_2 samples, respectively. The Gaussian fitting in Fig. 6a presents five emission peaks at 470, 496, 525, 560, and 590 nm, indicating the co-emission of transitions involving different defects in ZnO structure [32–35]. It is reported that the origin of the visible emissions in ZnO is still highly controversial, and various defect centers are responsible for green, yellow, and red

emissions [32–35]. The blue-green emissions at 470, 496, and 525 nm originated from oxygen vacancy (V_O) [33], singly charged oxygen vacancy (V+O) [34], doubly charged oxygen vacancy (V_O^{++}) [32], oxygen antisites (O_a) and zinc vacancy (V_{Zn}) [35]. The yellow peaks at 560 and 590 nm possibly contributed to interstitial oxygen defect O_i [35].

For the ZnO/MoS_2 heterostructures nanowires, the Gaussian fitting Figure 6b reveals six different peaks at 470, 501, 534, 570, 597, and 618 nm. Similar to the case of the ZnO nanowires, the blue-green emissions at 470, 501, and 534 nm are related to oxygen vacancies, and the yellow emissions at 570 and 597 nm are associated with interstitial oxygen defect Oi [32]. Compared with the visible peaks of ZnO nanowires, there is a redshift toward a higher wavelength of the visible emission peaks of ZnO/MoS_2 heterostructures, probably due to the changes in the local environments surrounding the defect centers [9]. It could be related to the strained lattice [11] and the evolution of defects states [36] due to the mismatch between the primitive cell of ZnO and MoS_2. Moreover, the occurrence of a new orange-red emission at 618 nm could be identified. It could be related to excess oxygen atoms located at interstitial sites of the ZnO/MoS_2 lattice. This result is consistent with the dominance of oxygen atoms in the ZnO/MoS_2 heterostructure, as demonstrated in Fig. 3b [9]. Here, it is worth noticing that no peak associated with the MoS_2 phase could be observed in the PL spectrum of the ZnO/MoS_2 heterostructures. This can be explained by the fact that MoS_2 is an indirect bandgap semiconductor exhibiting no room-temperature PL signal [9].

IV. CONCLUSION

In conclusion, ZnO nanowires and ZnO/MoS_2 heterostructure nanowires were successfully grown by a one-step evaporation method. The XRD patterns and Raman spectra demonstrate the existence of ZnO and MoS_2 phases in the ZnO/MoS_2 heterostructures. The diameters of ZnO/MoS_2 heterostructures are smaller than that of pure ZnO nanowires grown in the same experimental setup. PL and PLE studies reveal a considerable reduction in the intensity of the defect-related visible emissions of the ZnO/MoS_2 heterostructures. The observed visible emission PL intensity reduction has been explained due to the efficient passivation of the ZnO surface and interface defects by the MoS_2 layer. The strong optical absorption in the visible region of MoS_2 and the formation of ZnO/MoS_2 heterostructure with staggered type-II band alignment could also be the other causes of this reduction. The deconvolution of the visible emission of ZnO nanowires reveals 5 defect-related emissions, including V_O, V^+O, $V^{++}O$, oxygen antisite O_i, and V_{Zn}. Furthermore, the deconvoluted visible emission of the ZnO/MoS_2 heterostructures disclosed a new orange-red emission at 618 nm, next to the 5 emission peaks as observed for the ZnO sample. This orange-red emission is attributed to excess oxygen atoms located at the interstitial site of the ZnO/MoS_2 lattice.

ACKNOWLEDGMENTS

This research is funded by Vietnam National Foundation for Science and Technology Development (NAFOSTED) under grant number 103.02-2017.365.

REFERENCES

[1] A. B. Djuris and Y. H. Leung, *Optical properties of ZnO nanostructures*, *Small* **2** (2006) 944.

[2] P. Liang, B. Tai, H. Shu, T. Shen and Q. Dong, *Doping properties of MoS_2/ZnO (0001) heterojunction ruled by interfacial micro-struc- ture: from first principles*, *Solid State Commun.* **204** (2015) 67.

[3] K. Ueda, H. Tabata and T. Kawai, *Magnetic and electric properties of transition-metal-doped ZnO films*, *Appl. Phys. Lett.* **79** (2001) 988.

[4] J. R. Neal, A. J. Behan, R. M. Ibrahim, H. J. Blythe, M. Ziese, A. M. Fox and G. A. Gehring, *Room-temperature magneto-optics of ferromagnetic transition-metal-doped ZnO thin films*, *Phys. Rev. Lett.* **96** (2006) 1.

[5] L. Zhang, X. Ji, X. Ren, Y. Ma, X. Shi, Z. Tian, A.M. Asiri, L. Chen, B. Tang, X. Sun, *Electrochemical Ammonia Synthesis via Nitrogen Reduction Reaction on a MoS_2 catalyst: theoretical and experimental studies*, *Adv. Mater.* **30** (2018) 2.

[6] L. David, R. Bhandavat and G. Singh, *MoS_2/graphene composite paper for sodium-ion battery electrodes*, *ACS Nano* **8** (2014) 1759.

[7] M. A. Kang, S. J. Kim, W. Song, S. jin Chang, C.Y. Park, S. Myung, J. Lim, S.S. Lee, K.S. An, *Fabrication of flexible optoelectronic devices based on MoS_2/graphene hybrid patterns by a soft lithographic patterning method*, *Carbon N. Y.* **116** (2017) 167.

[8] M. Y. Lei, C. M. Liu, Y. G. Zhou, S. H. Yan, S. B. Han, W. Liu, X. Xiang and X. T. Zu, *Microstructure and photoluminescence of MoS_2 decorated ZnO nanorods*, *Chinese J. Phys.* **54** (2016) 51.

[9] H. Yu, C. M. Liu, X. Y. Huang and M. Y. Lei, *The microstructure and photoluminescence of ZnO–MoS_2 core shell nano-materials*, *Mater. Res. Express* **4** (2017) 015024.

[10] R. Selvaraj, K.R. Kalimuthu and V. Kalimuthu, *A type-II MoS_2/ZnO heterostructure with enhanced photocatalytic activity*, *Mater. Lett.* **243** (2019) 183.

[11] S. Wang, C. Ren, H. Tian, J. Yu and M. Sun, *MoS_2/ZnO van der Waals heterostructure as a high-efficiency water splitting photocatalyst: A first-principles study*, *Phys. Chem. Chem. Phys.* **20** (2018) 13394.

[12] H. Yu, C. M. Liu, X. Y. Huang and M. Y. Lei, *The microstructure and photoluminescence of ZnO-MoS_2 core shell nano-materials*, *Mater. Res. Express* **4** (2017) 015024.

[13] K. Zhang, Y. Zhang, T. Zhang, W. Dong, T. Wei, Y. Sun, X. Chen, G. Shen and N. Dai, *Vertically coupled ZnO nanorods on MoS_2 monolayers with enhanced Raman and photoluminescence emission*, *Nano Res.* **8** (2015) 743.

[14] E. Benavente, F. Durán, C. Sotomayor-Torres and G. González, Heterostructured layered hybrid ZnO/MoS_2 nanosheets with enhanced visible light photocatalytic activity, *J. Phys. Chem. Solids.* **113** (2018) 119.

[15] W. Jian, X. Cheng, Y. Huang, Y. You, R. Zhou, T. Sun and J. Xu, *Arrays of ZnO/MoS_2 nanocables and MoS_2 nanotubes with phase engineering for bifunctional photoelectrochemical and electrochemical water splitting*, *Chem. Eng. J.* **328** (2017) 474.

[16] X. Chang, X. Qiao, K. Li, P. Wang, Y. Xiong, X. Li, F. Xia and Q. Xue, *UV assisted ppb-level acetone detection based on hollow ZnO/MoS_2 nanosheets core/shell heterostructures at low temperature*, *Sens. Actuators B Chem.* **317** (2020) 128208.

[17] L. Ning, T. Jiang, Z. Shao, K. Ding, X. Zhang and J. Jie, *Light-trapping enhanced ZnO-MoS_2 core-shell nanopillar arrays for broadband ultraviolet-visible-near infrared photodetection*, *J. Mater. Chem. C* **6** (2018) 7077.

[18] D. Q. Trung, M. T. Tran, N. Tu, L. T. H. Thu, N. T. Huyen, N. D. Hung, D. X. Viet, N. D. T. Kien and P. T. Huy, *Synthesis, structural and optical properties of ZnS/ZnO heterostructure-alloy hexagonal micropyramids*, *Opt. Mater. (Amst).* **125** (2022) 1.

[19] D. Q. Trung, M. T. Tran, N. D. Hung, Q. Nguyen Van, N. T. Huyen, N. Tu and H. Pham Thanh, *Emission-tunable Mn-doped ZnS/ZnO heterostructure nanobelts for UV-pump WLEDs*, *Opt. Mater. (Amst)* **121** (2021) 111587.

[20] S. A. Khan, T. Khan, Zulfiqar and M. Khan, *Enhanced photoluminescence performance of MoS_2 nanostructures after amalgamation with ZnO NPs*, *Optik (Stuttg)* **220** (2020) 165201.

[21] X. Jia, Z. Lin, T. Zhang, B. Puthen-Veettil, T. Yang, K. Nomoto, J. Ding, G. Conibeer and I. Perez-Wurfl, *Accurate analysis of the size distribution and crystallinity of boron doped Si nanocrystals: Via Raman and PL spectra*, *RSC Adv.* **7** (2017) 34244.

[22] H. Xia, Y. L. He, L. C. Wang, W. Zhang, X. N. Liu, X. K. Zhang, D. Feng and H. E. Jackson, *Phonon mode study of Si nanocrystals using micro-Raman spectroscopy*, *J. Appl. Phys.* **78** (1995) 6705–6708.

[23] A. Báez-Rodríguez, L. Zamora-Peredo, M.G. Soriano-Rosales, J. Hernández-Torres, L. García-González, R.M. Calderón-Olvera, M. García-Hipólito, J. Guzmán-Mendoza and C. Falcony, *ZnO nanocolumns synthesized by chemical bath process and spray pyrolysis: Ultrasonic and mechanical dispersion of ZnO seeds and their effect on optical and morphological properties*, *J. Lumin.* **218** (2020) 116830

[24] R. Zhang, P.G. Yin, N. Wang and L. Guo, *Photoluminescence and Raman scattering of ZnO nanorods*, *Solid State Sci.* **11** (2009) 865.
[25] Z. Lei, J. Zhan, L. Tang, Y. Zhang and Y. Wang, *Recent development of metallic (1T) phase of molybdenum disulfide for energy conversion and storage*, *Adv. Energy Mater.* **8** (2018) 015024.
[26] A. A. Murthy, Y. Li, E. Palacios, Q. Li, S. Hao, J.G. Distefano, C. Wolverton, K. Aydin, X. Chen and V. P. Dravid, *Optically active 1D MoS_2 manobelts*, *ACS Appl. Mater. Interfaces* **10** (2018) 6799.
[27] X. Xu, C. Xu, Z. Shi, C. Yang, B. Yu and J. Hu, *Identification of visible emission from ZnO quantum dots: Excitation- dependence and size-dependence*, *J. App. Phys.* **111** (2012) 083521.
[28] B. Su, H. He and Z. Ye, *Large-area ZnO/MoS_2 heterostructure grown by pulsed laser deposition*, *Mater. Lett.* **253** (2019) 187.
[29] G. Faglia, M. Ferroni, T.T. le Dang, M. Donarelli, F. Rigoni and C. Baratto, *Vertically coupling ZnO nanorods onto MoS_2 flakes for optical gas sensing*, *Chemosensors* **8** (2020) 19.
[30] W. Mei, C. Chen, X. Chen, X. Liu, Z. Yang, F. Ding, Z. Chao and T. Liu, *Low-temperature construction of MoS_2 quantum dots/ZnO spheres and their photocatalytic activity under natural sunlight*, *J. Colloid Interface Sci.* **530** (2018) 714.
[31] X. Xu, S. Li, J. Chen, S. Cai, Z. Long, X. Fang, *Design principles and material engineering of ZnS for optoelectronic devices and catalysis*, *Adv. Funct. Mater.* **28** (2018) 1802029.
[32] B. Panigrahy, M. Aslam, D.S. Misra, M. Ghosh, D. Bahadur, Defect-related emissions and magnetization properties of ZnO Nanorods, *Adv. Funct. Mater.* **20** (2010) 1161.
[33] A. Van Dijken, E. A. Meulenkamp, D. Vanmaekelbergh and A. Meijerink, *The luminescence of nanocrystalline ZnO particles: the mechanism of the ultraviolet and visible emission*, *J. Lumin.* **89** (2000) 454.
[34] Z.G. Chen, A. Ni, F. Li, H. Cong, H.M. Cheng, G.Q. Lu, *Synthesis and photoluminescence of tetrapod ZnO nanostructures*, *Chem. Phys. Lett.* **434** (2007) 301.
[35] K. H. Tam, C. K. Cheung, Y.H . Leung, A. B. Djurišić, C. C. Ling, C. D. Beling, S. Fung, W. M. Kwok, W. K. Chan, D. L. Phillips, L. Ding and W. K. Ge, *Defects in ZnO nanorods prepared by a hydrothermal method*, *J. Phys. Chem. B* **110** (2006) 20865.
[36] H. Zeng, G. Duan, Y. Li, S. Yang, X. Xu and W. Cai, *Blue luminescence of ZnO nanoparticles based on non-equilibrium processes: Defect origins and emission controls*, *Adv. Funct. Mater.* **20** (2010) 561.